Pergamon

0301-9322(93)E0034-3

Int. J. Multiphase Flow Vol. 20, No. 2, pp. 383–396, 1994

0301-9322/94 $7.00 + 0.00

CONVECTION IN MULTIPLE LAYERS OF IMMISCIBLE LIQUIDS IN A SHALLOW CAVITY—I

STEADY NATURAL CONVECTION

A. PRAKASH and J. N. KOSTER†

Department of Aerospace Engineering Sciences, University of Colorado, Campus Box 429, Boulder, CO 80309, U.S.A.

(Received 23 November 1992; in revised form 12 August 1993)

Abstract—The problem of convective flow in multiple immiscible liquid layers in a differentially heated shallow rectangular cavity with rigid and insulated upper and lower boundaries is considered. As a model for multiple layers, a three-layer system featuring two non-deformable interfaces is investigated. The method of matched asymptotic expansions is used to determine the flow in the two distinct regions: the core region characterized by parallel flow; and the end-wall regions where flow turns around. The driving mechanism for convection is buoyancy. To study mechanical coupling across interfaces between immiscible liquids, the influence of varying encapsulant viscosity is investigated.

Key Words: natural convection, multiple immiscible layers, asymptotic theory

INTRODUCTION

During solidification of electronic materials, convective flow in the melt, especially time-dependent convective flow, can have undesirable effects on electronic properties of the solidified material. Pulling crystals of a volatile material, or a material with a volatile component, requires stringent control of the stoichiometry. To alleviate some of these problems, a technique which covers the surface of the material to be pulled with an amorphous liquid glass was developed. As a demonstration of the viability of this technique, germanium, PbTe and PbSe single crystals were encapsulated with molten B_2O_3 as the confining liquid (Metz *et al.* 1962). This new liquid encapsulation method has since been used to pull GaAs crystals (Johnson 1975). Recently the idea of liquid encapsulation was applied to float zone processing of GaAs in space (Barocela & Jalilevand 1987).

The development of improved crystal growth techniques has inspired the study of convection fluid physics in multiple liquid layers. In order to provide timely fluid mechanics data, several scientists have studied basic fluid dynamics of differentially heated immiscible double liquid layers with heating parallel to the interfaces.

Villers & Platten (1988, 1990) performed a one-dimensional analysis of convective flow in a two-layer system. They assume that in both layers a parallel flow develops in the mid-section of the cavity, where vertical velocities are zero. A key assumption in their analysis is that the temperature gradient across the cavity is constant. Prakash *et al.* (1993; Prakash & Koster 1993) performed a one-dimensional analysis of a mechanically decoupled "free–free" single liquid layer and of three immiscible layers using the same assumptions as Villers & Platten (1990). Wang *et al.* (1991) performed a one-dimensional analysis to investigate the differentially heated infinite two-layer system with constant heat flux end-wall conditions. Ramachandran (1990) and Doi & Koster (1993) utilized finite-difference algorithms and Fontaine & Sani (1992) used the finite-element computer code FIDAP to simulate the flow in two immiscible liquid layers with a free surface. Viviani & Golia (1992) studied Stokes flow in two rigidly contained immiscible liquid layers featuring one (liquid–liquid) interface.

†Author for correspondence.

The multiple liquid layer problem is an extension of the extensively studied problem of natural convection in a differentially heated cavity with one liquid, which is either completely confined or features a free surface. The names of Batchelor (1954) and Gill (1966) are associated with the earliest analytical investigations. Numerous investigators have studied this "cavity" problem numerically. We refer to the calculations of DeVahl Davis (1968) and Carpenter & Homsy (1989) for an extensive bibliography.

For shallow cavities, with height much smaller than length (aspect ratios $d/l \ll 1$), direct numerical modeling of the flow becomes expensive. However, analytical progress is possible with asymptotic methods. Batchelor (1954) considered the problem of a single liquid for both small and large Grashof numbers (Gr). For small Gr, his solution is an asymptotic expansion about the purely conductive, constant temperature gradient solution. For large Gr, he predicts an isothermal core, with thin boundary layers along all four sides. Gill (1966) studied the large Gr problem for the case of large aspect ratios ($d/l \gg 1$). He predicts a flow with thin boundary layers along the heated side walls where almost all the temperature drop occurs, and a core region where temperature is not isothermal as in Batchelor's solution, but is a function of the vertical coordinate.

The problem of convection in a shallow cavity with $d/l \ll 1$ was exhaustively investigated by Cormack *et al.* (1947a, b) and Imberger (1974), hereafter referred to as CLI. In part I of their investigation, they present an asymptotic theory valid in the limit $d/l \to 0$, with a fixed Gr. Experimental and numerical results presented in parts II and III of their investigation show excellent agreement with theory. CLI showed that convective flow in a shallow rectangular cavity can be divided into three, horizontally adjacent regions: the central, or "core", region; and the two end regions where flow turns around.

Flow in the core region is shown to be parallel to the interfaces, i.e. the vertical velocity components are zero. Also, the horizontal temperature profile in the core region is linear at all vertical locations. Therefore, the entire temperature drop occurs across the core region and the end regions serve to turn the flow around and play a passive role with regard to heat transfer. This is in contrast to the case where most of the temperature drop occurs in the vertical thermal boundary layers at the end walls, while the horizontal temperature gradient in the core region is small and negligible.

We utilize CLI's theory to study natural convection in three immiscible liquid layers, excluding thermocapillary effects. Three liquid layers are considered to be representative of a multiple-layer system. The theory can be easily extended to four or more layers, although the physical features of mechanical coupling between layers will not be significantly altered. Thermocapillary effects are discussed in the companion paper (Prakash & Koster 1994, this issue, pp. 397–414).

The multiple-layer problem is characterized by mechanical and thermal coupling across liquid interfaces. Mechanical coupling between liquid layers occurs due to the transfer of momentum across the interfaces. Transfer of momentum occurs via the continuity of the interface tangential velocity and the balance of shear stress across the interface. Together these two conditions comprise the "no-slip" condition at a liquid–liquid interface. It is this coupling between liquid layers that distinguishes this analysis from that of CLI.

MATHEMATICAL FORMULATION

We consider the fluid dynamics of a system of three immiscible liquid layers in a shallow (aspect ratio $d/l \ll 1$), rectangular, two-dimensional cavity. The cavity has length l and d is the height of the middle layer. The three layer heights are not necessarily equal. However, they are all of the same order, and each layer aspect ratio is considered small. The cavity height is, therefore, of order $3d$, which is considered to be much smaller than the cavity length. The cavity is differentially heated from the side, while the top and bottom boundaries are rigid and thermally insulated. A sketch of the geometry being considered is shown in figure 1. Convective flow results from horizontal differential heating, which produces a temperature gradient parallel to the two interfaces, while gravity is oriented perpendicular to the interfaces. Deformation of the interfaces is considered to be negligible in terrestrial gravity because of the strong stabilizing influence of hydrostatic forces, particularly for the weak convective flows considered here. This assumption is justified by

experiments on buoyancy-induced convective flow by Nataf *et al.* (1988), who did not observe significant interfacial deformations.

The governing equations of fluid flow in each liquid layer with the Boussinesq approximation, and the introduction of a stream function (ψ) and vorticity (ω) are:

$$\frac{\partial(\omega, \psi)}{\partial(x, y)} = \nu\nabla^2\omega + g\alpha\frac{\partial T}{\partial x}, \quad [1]$$

$$\frac{\partial(\theta, \psi)}{\partial(x, y)} = \kappa\nabla^2\theta \quad [2]$$

and

$$\nabla^2\psi = -\omega, \quad [3]$$

where θ is temperature and ν, κ and α are the kinematic viscosity, the thermal diffusivity and the coefficient of thermal expansion of the fluid, respectively. The acceleration due to gravity is g, and the bracket-operator (. .) is defined as

$$\frac{\partial(A, B)}{\partial(x, y)} \equiv \frac{\partial A}{\partial x}\frac{\partial B}{\partial y} - \frac{\partial A}{\partial y}\frac{\partial B}{\partial x}. \quad [4]$$

The governing equations for each layer are scaled using the thermophysical properties of the middle layer, and the applied temperature difference ΔT. The length of the cavity l and the middle-layer height d are used to scale the x and y coordinates, respectively. The continuity equation suggests that the appropriate vertical velocity scale is $v \sim (d/l)u$. The following velocity, length and temperature scales are used:

$$u^* = \left(\frac{g\alpha\Delta T d^2}{\nu}\right)\left(\frac{d}{l}\right)u; \quad v^* = \left(\frac{g\alpha\Delta T d^2}{\nu}\right)\left(\frac{d}{l}\right)^2 v \quad [5]$$

and

$$x^* = lx; \quad y^* = dy; \quad T^* = \Delta T\theta. \quad [6]$$

Using this scaling, the non-dimensional governing equations in a layer [i = t (top), m (middle), or b (bottom)] become

$$\mathrm{Gr}A^2\frac{\partial(\omega^i, \psi^i)}{\partial(x, y)} = \nu^i\left(A^2\frac{\partial^2\omega^i}{\partial x^2} + \frac{\partial^2\omega^i}{\partial y^2}\right) + \alpha^i\frac{\partial\theta^i}{\partial x}, \quad [7]$$

$$A^2\frac{\partial^2\psi^i}{\partial x^2} + \frac{\partial^2\psi^i}{\partial y^2} = -\omega^i \quad [8]$$

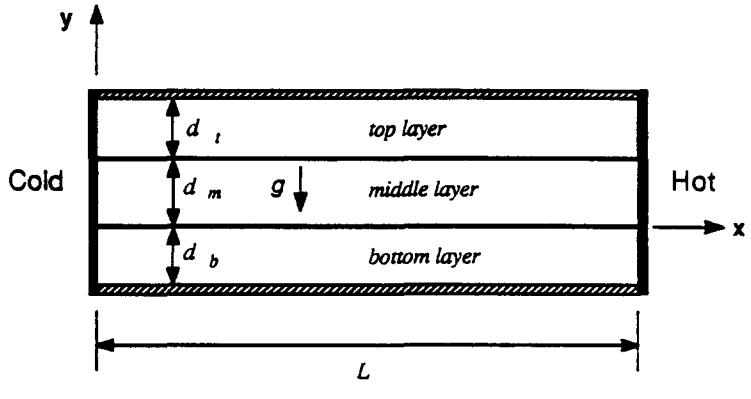

Figure 1. Sketch of the shallow cavity with three immiscible liquid layers.

and

$$\mathrm{GrPr}A^2\frac{\partial(\theta^i,\psi^i)}{\partial(x,y)}=\kappa^i\left(A^2\frac{\partial^2\theta^i}{\partial x^2}+\frac{\partial^2\theta^i}{\partial y^2}\right), \quad [9]$$

where the non-dimensional parameters, based on the middle-layer thermophysical properties, the middle-layer height d and the cavity length l, are defined as

$$\mathrm{Gr}=\frac{g\alpha\Delta Td^3}{\nu^2};\quad \mathrm{Pr}=\frac{\nu}{\kappa};\quad \mathrm{Ra}=\mathrm{GrPr}=\frac{g\alpha\Delta Td^3}{\nu\kappa};\quad A=\frac{d}{l}. \quad [10]$$

The parameters Gr, Pr, Ra and A refer to the Grashof number, the Prandtl number, the Rayleigh number and the aspect ratio, respectively. Capitalized superscripts are used to denote ratios of the thermophysical properties of the top (t) and bottom (b) layers with respect to the middle (m) layer, i.e.

$$\nu^{\mathrm{B}}=\frac{\nu_{\mathrm{b}}}{\nu_{\mathrm{m}}};\quad \nu^{\mathrm{T}}=\frac{\nu_{\mathrm{t}}}{\nu_{\mathrm{m}}}. \quad [11]$$

Ratios of other thermophysical properties and layer heights are denoted similarly.

The boundary condition at the four rigid side walls is the no-slip condition. A zero heat flux condition applies at the insulated top and bottom boundaries. At the cold and hot side walls an isothermal condition applies. These conditions take the form:

$$\text{at } y=-d^{\mathrm{B}},\quad \psi^{\mathrm{b}}=\psi^{\mathrm{b}}_y=\theta^{\mathrm{b}}_y=0;\qquad \text{at } y=1+d^{\mathrm{T}},\quad \psi^{\mathrm{t}}=\psi^{\mathrm{t}}_y=\theta^{\mathrm{t}}_y=0; \quad [12]$$

and

$$\text{at } x=0,\qquad \psi=\psi_x=0,\quad \theta=0;\quad \text{at } x=1,\qquad \psi=\psi_x=0,\quad \theta=1. \quad [13]$$

At the two interfaces, the no-slip conditions are a continuity of horizontal and vertical velocity and tangential shear. Also, temperature and heat flux are continuous across the interfaces. The interfacial boundary conditions are:

at $y=0$,

$$\mu^{\mathrm{B}}(\psi^{\mathrm{b}}_{yy}-A^2\psi^{\mathrm{b}}_{xx})=(\psi^{\mathrm{m}}_{yy}-A^2\psi^{\mathrm{m}}_{xx});\quad \psi^{\mathrm{b}}_x=\psi^{\mathrm{m}}_x=0;\quad \psi^{\mathrm{b}}_y=\psi^{\mathrm{m}}_y; \quad [14]$$

$$\theta^{\mathrm{b}}=\theta^{\mathrm{m}};\quad \lambda^{\mathrm{B}}\theta^{\mathrm{b}}_y=\theta^{\mathrm{m}}_y \quad [15]$$

and

at $y=1$,

$$\mu^{\mathrm{T}}(\psi^{\mathrm{t}}_{yy}-A^2\psi^{\mathrm{t}}_{xx})=(\psi^{\mathrm{m}}_{yy}-A^2\psi^{\mathrm{m}}_{xx});\quad \psi^{\mathrm{t}}_x=\psi^{\mathrm{m}}_x=0;\quad \psi^{\mathrm{t}}_y=\psi^{\mathrm{m}}_y; \quad [16]$$

$$\theta^{\mathrm{t}}=\theta^{\mathrm{m}};\quad \lambda^{\mathrm{T}}\theta^{\mathrm{t}}_y=\theta^{\mathrm{m}}_y; \quad [17]$$

where λ is the thermal conductivity of the referred liquid.

Our objective is to solve the above system of equations in each of the three layers with the applicable boundary conditions in the limit $A\to 0$.

Flow in the Core Region

The stream function is expanded using the small parameter A as follows:

$$\psi^i=\psi^i_0+A\psi^i_1+A^2\psi^i_2+\cdots. \quad [18]$$

Similarly, the vorticity ω and the temperature θ are also expanded using the small parameter A. An ordered set of equations is obtained by substituting the field variable expansions into the governing equations. General solutions of the ordered set of equations lead to a parallel flow in the core region at all orders:

$$\psi^i(x,y)=K^i_1\left(\frac{\alpha^i}{\nu^i}\right)f^i(y) \quad [19]$$

and

$$\theta^i(x,y)=K^i_1x+K^i_2+\mathrm{GrPr}(K^i_1)^2\frac{\alpha^i}{\kappa^i\nu^i}A^2g^i(y), \quad [20]$$

where

$$K_1^i = C_1^i + AC_2^i + A^2C_3^i + A^3C_4^i + \cdots \quad [21]$$

and

$$K_2^i = C_1^{*i} + AC_2^{*i} + A^2C_3^{*i} + A^3C_4^{*i} + \cdots, \quad [22]$$

and

$$f^i(y) = \left(\frac{y^4}{24} + A_4^i\frac{y^3}{6} + A_3^i\frac{y^2}{2} + A_2^i y + A_1^i\right) \quad [23]$$

and

$$g^i(y) = \left(\frac{y^5}{120} + A_4^i\frac{y^4}{24} + A_3^i\frac{y^3}{6} + A_2^i\frac{y^2}{2} + A_1^i y + A_0^i\right). \quad [24]$$

The 12 constants A_1^i to A_4^i are determined by satisfying the boundary conditions on the streamfunction. The temperature continuity boundary conditions require that

$$K_1^i = K_1; \quad K_2^i = K_2, \quad [25]$$

$$A_0^b = A_0^m \equiv 0 \quad [26]$$

and

$$A_0^t = \frac{\nu^T\kappa^T}{\alpha^T}\left(\frac{1}{120} + \frac{A_4^m}{24} + \frac{A_3^m}{6} + \frac{A_2^m}{2} + A_1^m\right) - \left(\frac{1}{120} + A_4^t + \frac{A_3^t}{6} + \frac{A_2^t}{2} + A_1^t\right). \quad [27]$$

The coefficients C_n and C_n^* must be determined by matching the core solution with the end-wall solution. A relationship between C_n and C_n^* can, however, be found by using the symmetry property

$$\frac{1}{D}\int_{-d^B}^{1+d^T} \theta\left(\frac{1}{2}, y\right) dy = \frac{1}{2}, \quad [28]$$

where D is the total non-dimensional depth of the system:

$$D = d^B + 1 + d^T. \quad [29]$$

This leads to

$$\left(\frac{K_1}{2} + K_2\right) + \mathrm{GrPr}\frac{(K_1)^2}{D}\sum_i\left[\frac{\alpha^i}{\nu^i\kappa^i}A^2\int_{y^{-i}}^{y^{+i}} g^i(y)\,dy\right] = \frac{1}{2}, \quad [30]$$

where y^{+i} and y^{-i} are the limits of the upper and lower vertical position for each layer (i). Therefore,

$$\frac{C_1}{2} + C_1^* = \frac{1}{2}; \quad C_2 = -2C_2^*; \quad C_3^* = -\frac{C_3}{2} - \mathrm{GrPr}\frac{(C_1)^2}{D}\sum_i\left[\frac{\alpha^i}{\nu^i\kappa^i}\int_{y^{-i}}^{y^{+i}} g^i(y)\,dy\right] \quad [31]$$

and

$$C_4^* = -\frac{C_4}{2} - \mathrm{GrPr}\frac{2C_1C_2}{D}\sum_i\left[\frac{\alpha^i}{\nu^i\kappa^i}\int_{y^{-i}}^{y^{+i}} g^i(y)\,dy\right]. \quad [32]$$

Flow in the End Region

To capture the flow pattern in the end regions, we stretch the coordinates in the vicinity of the cold wall as follows:

$$\xi = \frac{x}{A}; \quad \eta = y. \quad [33]$$

With this coordinate transformation, the governing equations become

$$\mathrm{Gr}\, A^2 \frac{\partial(\omega^i, \psi^i)}{\partial(\xi, \eta)} = \nu^i A \nabla^2 \omega^i + \alpha^i \frac{\partial \theta^i}{\partial \xi}, \quad [34]$$

$$\nabla^2 \psi^i = -\omega^i \quad [35]$$

and

$$\mathrm{GrPr}\, A \frac{\partial(\theta^i, \psi^i)}{\partial(\xi, \eta)} = \kappa^i \nabla^2 \theta^i. \quad [36]$$

In the end-wall regions, the wall boundary conditions must be satisfied and the solution must match the core flow away from the walls. As with the core region, the governing field variables in the end regions are also expanded using the small parameter A. Solutions at the two end walls will be similar, therefore we restrict ourselves to the solution near the cold wall ($\xi = 0; \theta = 0$).

Solution at O(1)

Substituting the expansion into the governing equations leads, at $O(1)$, to:

$$\nabla^2 \theta_0^i = 0; \quad \frac{\partial \theta_0^i}{\partial \xi} = 0. \quad [37]$$

In addition to satisfying the boundary conditions, the solution must match the core solution, which requires that

as $\xi \mapsto \infty$,

$$\theta_0^i = C_i^*. \quad [38]$$

The only possible solution satisfying [37], the boundary conditions and the matching condition is

$$C_1^* = 0; \Rightarrow \theta_0^i = 0. \quad [39]$$

This also implies that $C_1 = 1$.

Solution at O(A)

Using the $O(1)$ solution, the governing equation for temperature at $O(A)$ becomes

$$\nabla^2 \theta_1^i = 0. \quad [40]$$

The matching condition at this order is

as $\xi \mapsto \infty$,

$$\theta_1^i = C_1 \xi + C_2^*. \quad [41]$$

In order to satisfy the boundary conditions and the matching condition,

$$C_2^* = 0; \Rightarrow \theta_1^i = C_1 \xi = \xi. \quad [42]$$

With this $O(A)$ solution for temperature, the governing equations for the stream function and vorticity become:

$$\nabla^4 \psi_0^i = \frac{\alpha^i}{\nu^i}; \quad \omega_0^i = -\nabla^2 \psi_0^i. \quad [43]$$

These equations are to be solved with the previously defined boundary conditions and the following matching condition:

as $\xi \mapsto \infty$,

$$\psi_0^i = C_1 \frac{\alpha^i}{\nu^i} f^i(\eta) = \frac{\alpha^i}{\nu^i} f^i(\eta); \quad \psi_{0_\xi}^i = 0. \quad [44]$$

The biharmonic equation [43], with the boundary conditions and the matching conditions, is solved numerically.

Solution at $O(A^2)$

In order to make numerical computations independent of Gr and Pr, it is convenient to introduce the following notation:

$$\theta_2^i = \mathrm{GrPr}\,\theta_2'^i. \tag{45}$$

Upon substitution of the lower-order solutions, the governing equation for temperature at this order becomes

$$\nabla^2\theta_2'^i = \frac{1}{\kappa^i}\frac{\partial\psi_0^i}{\partial\eta}. \tag{46}$$

The matching condition for θ_2 is
as $\xi \mapsto \infty$,

$$\theta_2^i = C_3^* + \mathrm{GrPr}(C_1)^2\frac{\alpha^i}{\kappa^i\nu^i}g^i(\eta). \tag{47}$$

The constant C_3^* is unknown and is to be determined. Therefore, the following condition is imposed instead:
as $\xi \mapsto \infty$,

$$\frac{\partial\theta_2^i}{\partial\xi} = 0. \tag{48}$$

The harmonic problem for θ_2 with the previously defined boundary conditions and the above matching condition, is solved numerically. Using the solution for θ_2, the constant C_3^* is determined by integrating [47] as follows:

$$C_3^* = \frac{1}{D}\sum_i\left[\int_{\eta^{-i}}^{\eta^{+i}}\theta_2^i\,\mathrm{d}\eta - \mathrm{GrPr} - \frac{\alpha^i}{\nu^i\kappa^i}\int_{\eta^{-i}}^{\eta^{+i}}g(\eta)\,\mathrm{d}\eta\right]. \tag{49}$$

Therefore, from [31],

$$C_3 = \frac{-2\mathrm{GrPr}}{D}\sum_i\left(\int_{\eta^{-i}}^{\eta^{+i}}\theta_2^i\,\mathrm{d}\eta\right). \tag{50}$$

Integrating [46] over the depth of the cavity and using the rigid and insulated boundary conditions at the top and bottom leads to:

$$\frac{\partial^2}{\partial\xi^2}\sum_i\left(\int_{\eta^{-i}}^{\eta^{+i}}\theta_2'^2\,\mathrm{d}\eta\right) = 0. \tag{51}$$

This differential equation is solved with the following boundary conditions obtained from [13] and [50]:
at $\xi = 0$,

$$\sum_i\left(\int_{\eta^{-i}}^{\eta^{+i}}\theta_2'^i\,\mathrm{d}\eta\right) = 0 \tag{52}$$

and
as $\xi \mapsto \infty$,

$$\sum_i\left(\int_{\eta^{-i}}^{\eta^{+i}}\theta_2'^i\,\mathrm{d}\eta\right) = -C_3\frac{D}{2\mathrm{GrPr}}. \tag{53}$$

The only possible solution is

$$\sum_i\left(\int_{\eta^{-i}}^{\eta^{+i}}\theta_2'^i\,\mathrm{d}\eta\right) = 0 \quad \text{with } C_3 \equiv 0. \tag{54}$$

Therefore,

$$C_3^* = -\mathrm{GrPr}\frac{\alpha^i}{\nu^i\kappa^i}\int_{\eta^{-i}}^{\eta^{+i}}g(\eta)\,\mathrm{d}\eta. \tag{55}$$

Next, we proceed to the solution for ψ_1. As before, for convenience and to make the numerical computations independent of Gr and Pr, we introduce the following notation:

$$\psi_1^i = \mathrm{GrPr}\,\psi_1'^i + \mathrm{Gr}\,\psi_1'''^i. \tag{56}$$

With this notation, the governing equation for ψ_1 leads to the following two problems:

$$\nabla^4\psi_1'^i = \frac{\alpha^i}{\nu^i}\frac{\partial\theta_2'^i}{\partial\xi}; \quad \nabla^4\psi_1'''^i = -\frac{1}{\nu^i}\frac{\partial(-\nabla^2\psi_0^i, \psi_0^i)}{\partial(\xi,\eta)}. \tag{57}$$

The matching condition for ψ_1 using previously obtained results is
as $\xi \mapsto \infty$,

$$\psi_1^i = 0; \quad \psi_{1\xi}^i = 0. \tag{58}$$

The two biharmonic problems with homogeneous boundary conditions are solved numerically.

Solution at $O(A^3)$

As before, we introduce the following notation to make the solution independent of Gr and Pr:

$$\theta_3^i = \mathrm{Gr}^2\mathrm{Pr}^2\,\theta_3'^i + \mathrm{Gr}^2\mathrm{Pr}\,\theta_3'''^i \tag{59}$$

and

$$C_4 = \mathrm{Gr}^2\mathrm{Pr}^2\,C_4' + \mathrm{Gr}^2\mathrm{Pr}\,C_4''. \tag{60}$$

Using the lower-order solutions and the above notation, the governing equation for θ_3 leads to the following two harmonic problems:

$$\nabla^2\theta_3'^i = \frac{1}{\kappa^i}\left[\frac{\partial\psi_1'^i}{\partial\eta} + \frac{\partial(\theta_2'^i, \psi_0^i)}{\partial(\xi,\eta)}\right]; \quad \nabla^2\theta_3'''^i = \frac{1}{\kappa^i}\frac{\partial\psi_1'''^i}{\partial\eta}. \tag{61}$$

The corresponding matching conditions are
as $\xi \mapsto \infty$,

$$\theta_3'^i = -\frac{C_4'}{2}; \quad \theta_3'''^i = -\frac{C_4''}{2}. \tag{62}$$

As the two constants are unknown, for the numerical solution we use the following conditions:
as $\xi \mapsto \infty$,

$$\theta_{3\xi}'^i = 0; \quad \theta_{3\xi}'''^i = 0. \tag{63}$$

The two harmonic problems are solved numerically. In a similar fashion as for C_3, we find that

$$C_4'' = 0. \tag{64}$$

C_4' is determined numerically.

Next, we proceed to find the solution for ψ_2. For simplification, we introduce the following notation:

$$\psi_2^i = \mathrm{Gr}^2\mathrm{Pr}^2\,\psi_2'^i + \mathrm{Gr}^2\mathrm{Pr}\,\psi_2'''^i + \mathrm{Gr}^2\,\psi_2''''^i. \tag{65}$$

With the above notation and results, the governing equation for ψ_2 leads to the following three problems:

$$\nabla^4\psi_2'^i = \frac{\alpha^i}{\nu^i}\frac{\partial\theta_3'^i}{\partial\xi}, \tag{66}$$

$$\nabla^4\psi_2'''^i = \frac{\alpha^i}{\nu^i}\frac{\partial\theta_3'''^i}{\partial\xi} - \frac{1}{\nu^i}\left[\frac{\partial(\omega_0^i, \psi_1'^i)}{\partial(\xi,\eta)} + \frac{\partial(\omega_1'^i, \psi_0^i)}{\partial(\xi,\eta)}\right] \tag{67}$$

and

$$\nabla^4 \psi_2'''^i = -\frac{1}{\nu^i}\left[\frac{\partial(\omega_0^i, \psi_1'''^i)}{\partial(\xi,\eta)} + \frac{\partial(\omega_1'''^i, \psi_0^i)}{\partial(\xi,\eta)}\right]. \quad [68]$$

The matching condition for ψ_2 is

as $\xi \mapsto \infty$,

$$\psi_2^i = C_3 \frac{\alpha^i}{\nu^i} f^i(\eta) = 0. \quad [69]$$

These three biharmonic problems with homogeneous boundary conditions are also solved numerically.

Since C_4 is not zero, the core-region solution is modified by end-wall effects at $O(A^3)$. For the expansion to be asymptotic, this term must be less than the first term in the expansion, which is unity. From this we obtain the following criteria:

$$A^3 \,\mathrm{Gr}^2\mathrm{Pr}^2 \ll \frac{1}{C_4'}. \quad [70]$$

Heat transfer across the cold end wall is characterized by the average Nusselt number Nu. Using the composite expansion for θ^i, we find the average Nu:

$$\mathrm{Nu} = 1 + A^2 \,\mathrm{Gr}^2\mathrm{Pr}^2 \frac{1}{D} \sum_i \left(\int_{\eta^{-i}}^{\eta^{+i}} \frac{\partial \theta_3'^i}{\partial \xi} \, \mathrm{d}\eta \right) + O(A^3). \quad [71]$$

Numerical Modeling

The finite-difference method is used to solve the harmonic and biharmonic problems. The harmonic problem is discretized using a 5-point operator providing $O(\delta^2)$ accuracy, while the biharmonic problem is discretized using a 13-point operator. The mesh is stretched along the horizontal (x)-direction using an exponential function, and it is stretched along the vertical (z)-direction using a cosine function in each layer. IMSL library routines are used to solve the resulting linear system of equations.

The calculations performed for this study assume all layers to be of equal height. We extend the end region horizontally towards the core a distance 5 times the middle-layer height. Therefore, the computational domain in non-dimensional space is 5.0 (horizontal) × 3.0 (vertical). The mesh in each layer is 51 × 51. Further refinement of the mesh was found to have an insignificant influence on the results.

RESULTS

The problem of buoyant convection in three immiscible layers in a shallow cavity is characterized by 15 parameters. These are height ratios, the 10 ratios of the thermophysical properties of the upper and lower layers with respect to the middle layer, the aspect ratio, the Gr and the Pr of the middle layer. For this investigation we select three systems which are composed of ethylene glycol encapsulated above by silicone oils (SO; 1, 10 and 100 cSt) and below by fluorinert liquids (FC-75, FC-70, FC-71). The thermophysical properties of these liquids are listed in table 1.

We select three combinations: (i) SO 10 cSt/ethylene glycol/FC-70; (ii) SO 1 cSt/ethylene glycol/FC-75; and (iii) SO 100 cSt/ethylene glycol/FC-71. The ratios of the thermophysical properties for these systems are listed in table 2. Case (i) represents "*equal*" *viscosity encapsulation*, i.e. encapsulant viscosities are the same order of magnitude as the middle layer. Case (ii) represents *low viscosity encapsulation*, i.e. encapsulant viscosities are an order of magnitude smaller than the middle layer. Case (iii) represents *high viscosity encapsulation*. The core-region flow in these systems has recently been investigated by Prakash & Koster (1993) Here, we concentrate on the flow in the cold end-wall region.

The "*equal*" *viscosity encapsulation* case is of interest because the driving forces for convection in the three layers are of comparable magnitude, as illustrated by the Gr values which are of

Table 1. Fluid properties

Fluids	Density (g/cm^3)	Kinematic viscosity (cm^2/s)	Dynamic viscosity (g/cm/s)	Thermal conduct. (W/cm-K)	Specific heat@25°C (J/g-K)	Thermal diffusivity (cm^2/s)	Coeff. of expansion $\times 10^5$ (1/K)	Pr
Ethylene glycol	1.11E + 00	1.54E − 01	1.72E − 01	2.58E − 03	2.39E + 00	9.67E − 04	6.20E − 04	1.59E + 02
FC-75	1.76E + 00	8.00E − 03	1.41E − 02	6.30E − 04	1.05E + 00	3.43E − 04	1.40E + 02	2.33E + 01
FC-70	1.94E + 00	1.34E − 01	2.60E − 01	7.00E − 04	1.05E + 00	3.44E − 04	1.00E + 02	3.89E + 02
FC-71	1.92E + 00	7.30E − 01	1.40E + 00	7.10E − 04	1.05E + 00	3.54E − 04	1.20E + 02	2.06E + 03
Dow 200-1.0	8.16E − 01	1.00E − 02	8.16E − 03	1.00E − 03	1.72E + 00	7.17E − 04	1.34E + 02	1.39E + 01
Dow 200-10.0	9.35E − 01	1.00E − 01	9.35E − 02	1.34E − 03	1.51E + 00	9.51E − 04	1.10E + 02	1.05E + 02
Dow 200-100.0	9.64E − 01	1.00E + 00	0.64E − 01	1.55E − 03	1.47E + 00	1.09E − 03	9.30E + 01	9.17E + 02

comparable magnitude in all three layers (see table 2). Streamlines and temperature profiles in the cold end-wall region are shown in figures 2(a) and (b). The criteria of [70] for this case becomes

$$A^3 \mathrm{Gr}^2\mathrm{Pr}^2 \ll 16{,}700 \qquad [72]$$

and the average Nu at the end wall is

$$\mathrm{Nu} = 1 + 4.941 \cdot 10^{-5} A^2 \mathrm{Gr}^2\mathrm{Pr}^2. \qquad [73]$$

The flow in the two encapsulant layers is very similar. But the flow in both encapsulants is much stronger than in the middle layer. The flow in the middle layer is partially entrained by the encapsulants. A weak buoyancy-induced roll, with downflow along the cold wall, forms at mid-height in the middle layer. This buoyancy roll is bounded by the counter-rotating non-symmetric flows induced by the encapsulant layers, and does not contact the encapsulant layers. The temperature in the middle layer remains in a nearly conductive state. In the vicinity of the end wall, isotherms are not orthogonal to the interfaces, therefore heat flows vertically across the interfaces. Away from the end walls, the isotherms become nearly orthogonal to the interfaces and the heat flow across the interfaces becomes negligible as the core region is approached.

For the *low viscosity encapsulation* case, the flow streamlines are shown in figure 3. The flow in both encapsulant layers is the characteristic buoyancy cell. The flow in the encapsulants is so strong that through mechanical coupling across the interfaces it completely entrains the middle layer. The buoyancy-induced flow in the middle layer is completely overcome, and a weak counter flow develops. The criteria of [70] for this case is

$$A^3 \mathrm{Gr}^2\mathrm{Pr}^2 \ll 65 \qquad [74]$$

and the average Nu at the end wall is

$$\mathrm{Nu} = 1 + 1.448 \cdot 10^{-2} A^2 \mathrm{Gr}^2\mathrm{Pr}^2. \qquad [75]$$

The temperature profile for this case is similar to that shown in figure 2(b) for the equal viscosity encapsulation case, and is very close to the conductive state.

Flow streamlines for the *high viscosity encapsulation* case are shown in figure 4. This case is of special interest due to its relevance to the encapsulated float zones where encapsulant liquids are significantly more viscous than the electronic melt. Strong buoyancy-driven flow is apparent in the middle layer. To satisfy continuity across interfaces, very thin interfacial rolls develop in the comparatively lower viscosity middle layer. The vertical extension of the lower interfacial roll is

Table 2. Ratios of the thermophysical properties

Two layers	Density ratio	Kinematic viscosity ratio	Dynamic viscosity ratio	Thermal conduct. ratio	Specific heat ratio	Thermal diffusivity ratio	Coeff. of expansion ratio	Pr ratio
SO 1cSt/Eth Gly	0.7325	0.0649	0.0476	0.3900	0.7178	0.7416	2.1613	0.0876
SO 10 cSt/Eth Gly	0.8393	0.6494	0.5450	0.5200	0.6303	0.9828	1.7742	0.6607
SO 100 cSt/Eth Gly	0.8654	6.4935	5.6192	0.6013	0.6163	1.1273	1.5000	5.7605
FC-70/Eth Gly	1.7415	0.8701	1.5153	0.2717	0.4377	0.3560	1.6129	2.4444
FC-71/Eth Gly	1.7235	4.7403	8.1699	0.2756	0.4377	0.3661	1.9355	12.9466
FC-75/Eth Gly	1.5799	0.0519	0.0821	0.2446	0.4377	0.3548	2.2581	0.1464

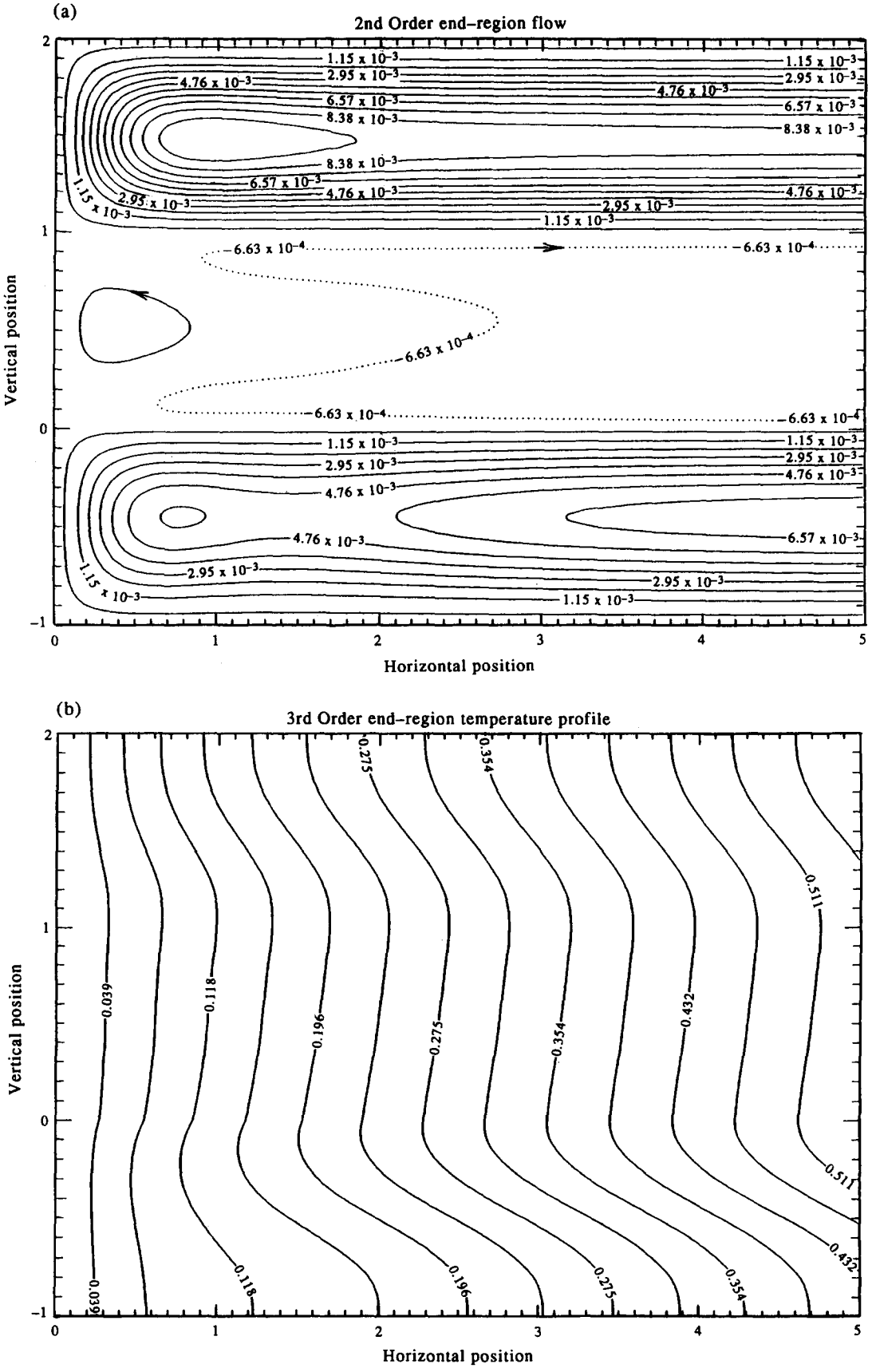

Figure 2. Equal viscosity encapsulation; $A = 0.1$, $\mathrm{Pr} = 159$, $\mathrm{Gr} = 0.5$: (a) second-order end-region flow; (b) third-order temperature profile in three layers.

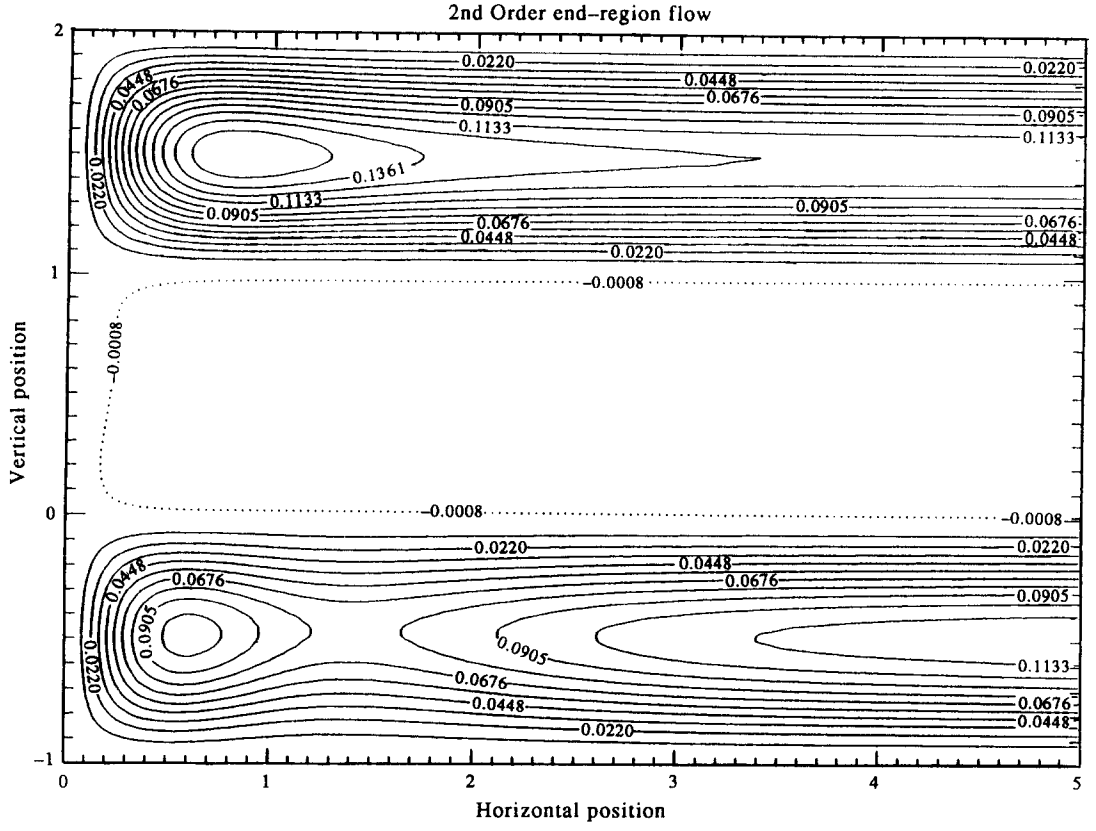

Figure 3. Low viscosity encapsulation; $A = 0.1$, Pr = 159, Gr = 7.0: second-order end-region flow.

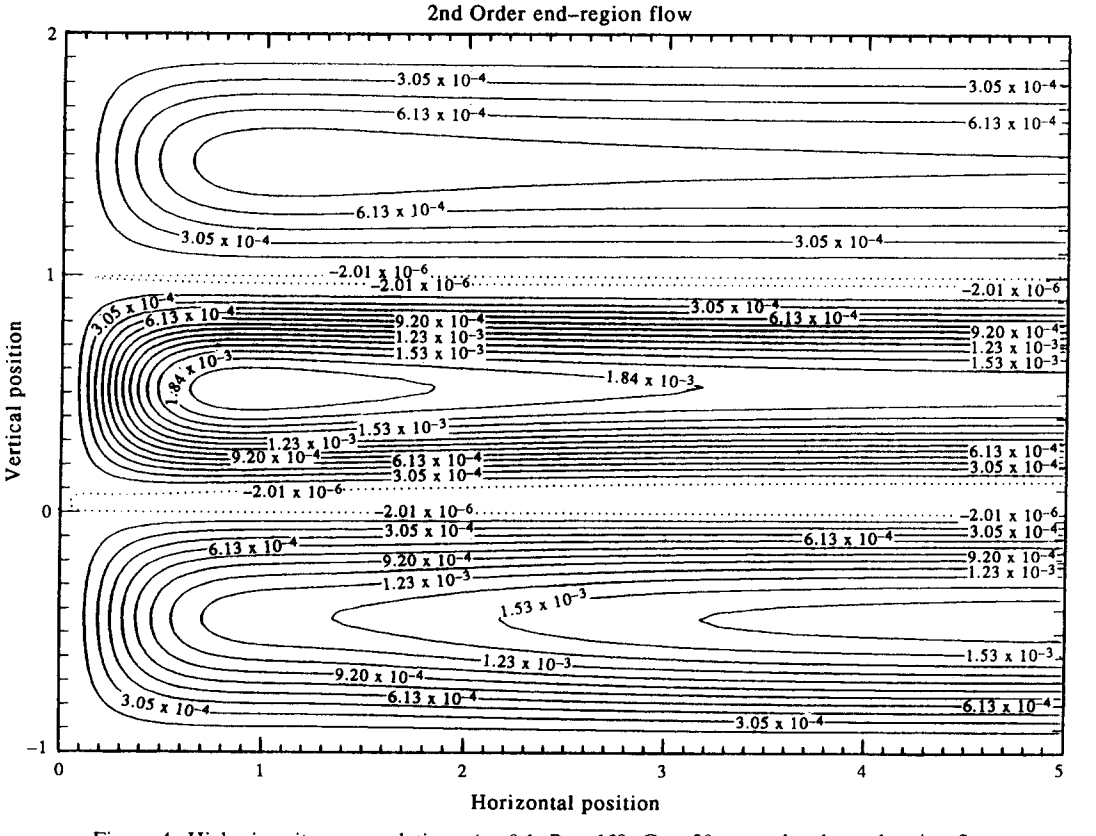

Figure 4. High viscosity encapsulation; $A = 0.1$, Pr = 159, Gr = 20: second-order end-region flow.

larger than the upper interfacial roll, reflecting the different viscosities of the encapsulants. Although the flow patterns in the two layers are different, the flow in both encapsulant layers is the characteristic buoyancy roll. An "eye" is detected in the upper layer and not in the lower layer. The criteria of [70] for this case is

$$A^3\,\mathrm{Gr}^2\mathrm{Pr}^2 \ll 270{,}000 \qquad [76]$$

and the average Nu at the end wall is

$$\mathrm{Nu} = 1 + 2.949 \cdot 10^{-6} A^2\,\mathrm{Gr}^2\mathrm{Pr}^2. \qquad [77]$$

The temperature distribution for this case is also similar to that shown in figure 2(b) for the equal viscosity encapsulation case, and is also very close to the conductive state.

CONCLUSION

The problem of convective flow in multiple immiscible liquid layers in a differentially heated shallow cavity with rigid and insulated upper and lower boundaries has been investigated. Cormack *et al.* (1974a) applied the method of matched asymptotic expansions to determine the convective flow in a differentially heated shallow cavity containing a single liquid. Flow in multilayer systems is determined by an extension of CLI's theory. We restrict this study to three distinct triple-layer systems.

In snallow cavities, with aspect ratios much smaller than unity, the temperature drop occurs through the core of the cavity, while the end regions play a passive role, and simply act to turn the flow around. In such cavities, the mechanical interaction of multiple liquid layers across the interfaces has been investigated. A criterion establishing the limits for this flow regime has been established for each of the three systems considered. This criterion and the ensuing flow patterns are strongly dependent on the thermophysical property ratios of the encapsulant liquids relative to the encapsulated liquid.

A comparison between CLI's solution for a single layer with rigid upper and lower boundaries and the encapsulated middle-layer solution shows that encapsulation is found to have a significant influence on the flow pattern and the heat transfer rate. The encapsulants provide asymmetric interfacial boundaries for the middle layer. Across these boundaries, the encapsulants and the middle layer are thermally and mechanically coupled. Thermal coupling between the layers lead to vertical heat transfer between the layers, particularly near the end walls. Mechanical coupling between the liquid layers results in a middle-layer flow which, depending on the encapsulant viscosities, is either completely entrained by the outer encapsulants and is counter to the buoyancy flow, or is comprised of as many as two or three recirculation cells. In contrast, CLI's flow solution is always composed of a single buoyancy recirculation cell.

As anticipated, the middle-layer flow with *high viscosity encapsulation* approaches CLI's single-layer flow. For the *high viscosity encapsulation* case, the heat transfer rate as depicted by the end-wall Nu also approaches that for CLI's single layer. With *low* and *"equal" viscosity encapsulation*, the middle-layer flow is entrained by the outer encapsulants. Entrainment of the middle layer is sufficiently strong that it overpowers the buoyancy flow. As buoyancy and entrainment effects compete in the middle layer, the flow in the middle layer is reduced. Although the aspect ratio and the Gr considered in this study are not directly relevant for crystal growth applications, results of this analysis indicate that liquid encapsulation has the potential to reduce convective flow in the encapsulated melt layer.

Acknowledgment—Support from NASA MSAD, under Grant NAG3-1094, for this study is greatly appreciated.

REFERENCES

BAROCELA, E. & JALILEVAND, A. 1987 Liquid encapsulated float zone method for microgravity production of gallium arsenide. AIAA paper 87-0390.

BATCHELOR, G. K. 1954 Heat transfer by free convection across a closed cavity between vertical boundaries at different temperatures. *Q. Appl. Math.* **12,** 209–233.

BATCHELOR, G. K. 1954 Heat transfer by free convection across a closed cavity between vertical boundaries at different temperatures. *Q. Appl. Math.* **12,** 209–233.

CARPENTER, B. & HOMSY, B. 1989 Combined buoyant–thermocapillary flow in a cavity. *J. Fluid Mech.* **207,** 121–132.

CORMACK, D. E., LEAL, L. G. & IMBERGER, J. 1974a Natural convection in a shallow cavity with differentially heated end walls, Part I. Asymptotic theory. *J. Fluid Mech.* **65,** 209–229.

CORMACK, D. E., LEAL, L. G. & SEINFELD, J. H. 1974b Natural convection in a shallow cavity with differentially heated end walls, Part II. Numerical solutions. *J. Fluid Mech.* **65,** 231–246.

DEVAHL-DAVIS, G. 1968 Natural convection of air in a square cavity—a benchmark numerical solution. *Int. J. Num. Meth. Fluids* **3,** 249–264.

DOI, T. & KOSTER, J. N. 1993 Marangoni convection in two immiscible liquid layers. *Phys. Fluids A: Fluid Dynam.* **5,** 1914–1927.

FONTAINE, J-P. & SANI, R. L. 1992 High Prandtl number fluids in a multilayered system under 1-g or μ-g environment. Report ESA SP-333, 197–202.

GILL, A. E. 1966 The boundary-layer regime for convection in a rectangular cavity. *J. Fluid Mech.* **26,** 515–536.

IMBERGER, J. 1974 Natural convection in a shallow cavity with differentially heated end walls, Part III. Experimental results. *J. Fluid Mech.* **65,** 247–260.

JOHNSON, E. S. 1975 Liquid encapsulated float zone melting of GaAs. *J. Cryst. Growth* **30,** 249–256.

METZ, E. P. A., MILLER, R. C. & MAZELSKY, R. 1962 A technique for pulling single crystals of volatile materials. *J. Appl. Phys.* **33,** 2016–2017.

NATAF, H. C., MORENO, S. & CORDIN, P. 1988 What is responsible for thermal coupling in layered convection? *J. Phys.-France* **49,** 1707–1714.

PRAKASH, A. & KOSTER, J. N. 1993 Natural and thermocapillary convection in three layers. *Eur. J. Mech. B/Fluids.* **12,** 635–655.

PRAKASH, A. & KOSTER, J. N. 1994 Convection in multiple layers of immiscible liquids in a shallow cavity—II. Steady thermocapillary convection. *Int. J. Multiphase Flow* **20,** 397–414.

PRAKASH, A., FUJITA, D. & KOSTER, J. N. 1993 Surface tension and buoyancy effects on a free–free layer. *Eur. J. Mech. B/Fluids* **12,** 15–29.

RAMACHANDRAN, N. 1990 Thermal buoyancy and Marangoni convection in a two fluid layered system—a numerical study. AIAA paper 90-0254.

VILLERS, D. & PLATTEN, J. K. 1988 Thermal convection in superposed immiscible liquid layers. *Appl. Scient. Res.* **45,** 145–152.

VILLERS, D. & PLATTEN, J. K. 1990 Influence of interfacial tension gradients on thermal convection in two superposed immiscible liquid layers. *Appl. Scient. Res.* **47,** 177–191.

VIVIANI, A. & GOLIA, C. 1992 Stokes flows in superimposed immiscible liquids with horizontal heating. Report IAF-92-0909.

WANG, C. H., SEN, M. & VASSEUR, P. 1991 Analytical investigation of Bénard-Marangoni convection heat transfer in a shallow cavity filled with two immiscible fluids. *Appl. Scient. Res.* **48,** 35–53.